The Canadian Mineralogist
Vol. 41, pp. 259-272 (2003)

A LASER PROBE COUPLED WITH ICP – DOUBLE-FOCUSING SECTOR-FIELD MASS SPECTROMETER FOR IN SITU ANALYSIS OF GEOLOGICAL SAMPLES AND U–Pb DATING OF ZIRCON

MASSIMO TIEPOLO[§], PIERO BOTTAZZI AND MARCO PALENZONA

C.N.R. – Istituto di Geoscienze e Georisorse – Sezione di Pavia, via Ferrata 1, I–27100, Pavia, Italy

RICCARDO VANNUCCI

C.N.R. – Istituto di Geoscienze e Georisorse – Sezione di Pavia, e Dipartimento di Scienze della Terra, Università di Pavia, via Ferrata 1, I–27100, Pavia, Italy

ABSTRACT

Quadrupole ICP–MS is currently the method of choice for laser-ablation applications, since sector-field instruments are generally considered too slow for the acquisition of rapidly varying signals. However, the new generation of double-focusing sector-field mass spectrometers is capable of rapidly scanning the mass spectrum both magnetically and electrostatically, and the combination of these two scan modes approaches the performance of quadrupoles for most practical applications. We present the instrumental configuration and operating conditions of a LA–ICP–MS system, assembled by coupling a 266 nm laser source to a double-focusing magnetic-sector mass spectrometer ("Element", Finnigan MAT). The capability of the adopted configuration to furnish high-quality *in situ* trace-element analysis of minerals and U–Pb geochronological data is described. Concentrations of thirty geochemically relevant elements (*LILE*, *HFSE*, *REE*, actinides) were determined on geological samples with good precision and accuracy (<10%), evaluated using two USGS basaltic glass reference materials, BCR–2 and BIR–1. The high sensitivity and low background allowed extremely low limits of detection (down to the ppb level) for the heaviest elements, and between 10 and 100 ppb for the lighter masses. The first results on U:Pb ratio determinations are also very positive. By adopting an external matrix-matched standard for corrections of mass bias and laser-induced fractionation of elements, precision and accuracy in age determinations to better than ~2% are attained on the zircon standard 91500.

Keywords: laser ablation, ICP–MS, double-focusing sector-field mass spectrometer, precision, accuracy, trace elements, U–Pb, zircon dating.

SOMMAIRE

Les appareils ICP–MS munis d'un quadrupole sont préférés de nos jours dans les applications faisant appel à l'ablation au laser (LA), parce que les appareils à secteurs partagés sont généralement considérés trop lents dans l'acquisition de signaux qui varient rapidement. Toutefois, avec la nouvelle génération de spectromètres de masse à secteurs partagés et à double foyer, nous sommes capables de balayer rapidement le spectre des masses à la fois selon les propriétés magnétiques et électrostatiques. La combinaison des deux modes de balayage se rapproche des quadrupoles en performance dans la plupart des applications pratiques. Nous présentons les détails de la configuration de l'instrument LA–ICP–MS et les conditions d'opération du système; nous avons couplé une source laser de 266 nm à un spectromètre de masse à secteurs magnétiques partagés et à double foyer ("Element", Finnigan MAT). Nous documentons la capacité du système configuré ainsi à effectuer des analyses de minéraux *in situ* de haute qualité pour les éléments traces, y compris pour les applications géochronologiques utilisant le système U–Pb. Nous présentons nos résultats à propos de trente éléments géochimiquement importants (éléments lithophiles légers, éléments à champ électrostatique élevé, terres rares, actinides) obtenus sur échantillons géologiques avec bonnes précision et justesse (<10%), par évaluation de deux étalons de verre basaltique de référence, USGS BCR–2 et BIR–1. La sensibilité élevée et le faible bruit de fond nous ont permis des seuils de détection extrêmement faibles (de l'ordre du ppb) pour les éléments les plus lourds, et entre 10 et 100 ppb pour les masses plus légères. Les premiers résultats portant sur la détermination du rapport U:Pb s'avèrent aussi très

§ *E-mail address*: tiepolo@crystal.unipv.it

positifs. Avec l'adoption d'un étalon externe à matrice identique pour les corrections de biais dans les masses et de fractionnement des éléments au site de l'ablation, nous obtenons une précision et une justesse supérieures à environ 2% dans les déterminations d'âge de l'étalon de zircon 91500.

(Traduit par la Rédaction)

Mots-clés: ablation au laser, analyse ICP–MS, spectromètre à double foyer et à secteurs partagés, précision, justesse, éléments traces, U–Pb, datation du zircon.

Introduction

Since the early 1990s, laser-ablation – inductively coupled plasma – mass spectrometry (LA–ICP–MS) has undergone rapid development and has become very competitive for Earth Science applications in terms of cost, detection limits, sample throughput and number of detectable elements.

The chemical analysis of minerals using LA–ICP–MS is particularly demanding because of their great variability in optical properties and composition, which affects the interaction of the laser beam with the sample. Efforts have been made to find the optimum characteristics of the laser beam to induce efficient ablation on the largest variety of minerals (Jackson 2001, Günther *et al.* 2000, Jeffries *et al.* 1998 and references therein).

Commercial ICP mass spectrometers have undergone a technological evolution that today gives the analyst a large choice of possible instruments and supplies. However, most analysts using laser ablation have adopted a quadrupole mass spectrometer. In the past, this choice has been almost compulsory, as laser-ablation sampling produces rapidly varying, transient signals, which require the scanning capability of the quadrupole mass analyzer. Single-collector sector-field mass spectrometers, in particular, are generally still considered too slow for the purpose, owing to the settling times required for the stabilization of the magnet after a mass jump. However, they also have some advantages relative to quadrupoles, that is, higher sensitivity, better abundance-sensitivity, the possibility to work at high mass-resolution, and the "flat-topped" aspect of peak shapes.

The new generation of double-focusing sector-field mass spectrometers, however, is capable of rapidly scanning the mass spectrum both magnetically and electrostatically, and the combination of these two scan modes approaches the performance of quadrupoles for most practical applications. These features make them suitable for coupling with laser-ablation microsamplers, competitive in principle to quadrupoles and potentially superior in some fields of application, as, for instance, the determination of isotope ratios. Nevertheless, the scarcity of results obtained with this instrumental configuration, so far uncommon in micro-analytical laboratories, leaves this potential largely untested. In this paper, we report the analytical results obtained at CNR–IGG–Pavia with a LA–ICP–MS system coupling a 266 nm Nd:YAG laser probe with a double focusing magnetic-sector mass spectrometer. We assess the performance of our instrument in terms of precision, accuracy and detection limits, in trace-element determinations, and present results of a preliminary study on U/Pb dating of zircon.

LA–ICP–MS Instrumental Configuration

Laser probe

The laser-ablation apparatus used compares well with that developed at Memorial University of Newfoundland by Jackson *et al.* (1992). A spatial filter is added for a better-homogenized laser beam. The laser source consists of a Q-switched Nd:YAG laser (Brilliant, Quantel), whose fundamental emission in the near-IR region (1064 nm) is converted into 266 nm by two harmonic generators. Using mirrors, the laser beam is carried into a petrographic microscope, focused above the sample, and then projected onto it. The laser power is controlled by an optical attenuator consisting of a rotatable zero-order half-wave plate, a high-power UV prism, and a beam dump. The configuration is similar to that described in Jeffries *et al.* (1998). Spatial filtering is attained by expanding the laser beam at the exit of the attenuator using a 3× beam expander. The expanded beam is subsequently diaphragmed (4–2 mm) by means of a MACOR® ring. The demagnification ratio used at the imaging position (pass length from aperture to objective / working distance of objective) is 46. This procedure allows the selection and transmission to the sample of only the most homogeneous part of the laser beam. The spot size can be varied by changing the sample position below the focus point of the laser or the diaphragm diameter. The 266 nm laser beam has a pulse width of 4.2 ns. Its maximum output energy of about 35 mJ/pulse is reduced by spatial filtering to about 1.0 mJ/pulse, which correspond to a maximum density of energy on the sample of 318 J/cm^2 and 20 J/cm^2 at a spot size of 80 μm and 20 μm, respectively.

Ablation cell and gas line

The "in-house-built" ablation cell is a cylinder with an internal volume of approximately 27 cm^3. The car-

rier gas enters through three apertures aligned at 60° each other and exits through a single, diametrically opposed output aperture. This configuration was found to allow the complete flooding of the internal surface and a rapid evacuation of the ablated material. Helium is used as the carrier gas; it is mixed, in proportion close to 1:1, with Ar downstream of the ablation cell in a T-tube, wherein the two gases enter oppositely and exit laterally, thus ensuring complete mixing. The whole gas line is made of TYGON® tubes with an internal diameter of 1.6 mm. In U–Pb determinations, a cylinder with an internal volume of 125 cm^3 is placed on the gas line before the ICP torch in order to achieve a smoothing of the signal. Two double-layer "Emflon" PTFE membrane filters (PALL®, Mini–Gaskleen Filter) having an absolute gas-removal rating of 0.003 μm, and placed on the gas line, allow a three-times reduction in Pb background signal. The Ar gas flows are controlled by the standard mass-flow controllers of the Element instrument. The He gas flow is regulated by an additional mass-flow controller of the same type (Manger & Wittmann, model WFC 022).

ICP–MS instrument and optimization

The ablated material is analyzed with a single-collector double-focusing sector-field ICP–MS (Element, Finnigan Mat, Bremen, Germany). The standard Element ICP torch was replaced by the Capacitive Decoupling torch (CD–2), which allows a normally pure inductive coupling, thus eliminating the secondary discharge between the ICP and the sampling cone of the mass spectrometer, and decreasing the spread in kinetic energy of the ion beam. Under wet plasma conditions, this torch ensures a gain in sensitivity of about 10 times (IGG–Pavia, unpublished data).

The ICP–MS alignment was initially performed using nebulization of standard solutions and then optimized for dry plasma with the laser probe. Fine alignment (optimum RF power and gas flows) is performed before every analytical session on the NIST 610 glass reference material by maximizing the signals of ^{139}La (^{208}Pb in U–Pb analyses) and ^{232}Th, and monitoring the ThO^+/Th^+ ratio in order to estimate the formation of polyatomic oxides. Optimum average instrumental operating conditions are summarized in Table 1. Under dry plasma conditions, a low RF power (about 800–900 W) is required to enhance the effect of the guard electrode in the Capacitive Decoupling torch. Using these operating conditions, the CD torch produces a signal about 4–5 times higher than the conventional torch. At low RF power, oxide formation is higher ($ThO^+/Th^+ \approx 0.9\%$) than with the conventional torch, but the oxide formation should not affect the determination of depleted and slightly enriched *LREE* patterns (Jackson *et al.* 1992). The reduction of the ThO^+/Th^+ ratio (down to 0.2%), necessary for the accurate determination of high-enrichment *LREE* patterns, can be achieved at hotter conditions in the plasma by increasing the RF power (about 1000 W) or decreasing the gas flows, but at the cost of lower sensitivity.

TABLE 1. ICP–MS OPERATING CONDITIONS

RF power	800–900 W		
Cooling gas	12.08 L/min	Auxiliary gas	1.00 L/min
Sample gas	0.9–1.1 L/min	Carrier gas	0.9–1.1 L/min

Data Acquisition

Element concentrations

The 34 masses of petrological interest between ^{25}Mg and ^{238}U that were selected for analysis are reported in Table 2. Isotope selection was performed on the basis of the best compromise between maximum isotopic abundance and the minimum presence of interference. Mass resolution was set to the low mode (nominally 300 $M/\Delta M$) because of the absence of relevant interferences

TABLE 2. ACQUISITION LIST PARAMETERS FOR TRACE-ELEMENT DETERMINATIONS

Element	Mass (a.m.u.)	Settling time (ms)	Sample time (ms)	Samples per peak	Segment duration (ms)	Mass window (%)	Type of acquisition	Total time (ms)
Mg	**25**	**80**	**3**	**3**	**15**	**160**	**Analog**	**95**
Si	29	2	1	8	14	160	Analog	16
Ca	**43**	**33**	**1**	**9**	**11**	**110**	**Both**	**44**
Ca	44	1	1	8	11	110	Analog	12
Sc	45	1	1	9	11	110	Both	12
Ti	49	1	1	9	11	110	Both	12
V	51	1	1	9	11	110	Both	12
Cr	53	1	1	9	11	110	Both	12
Rb	**85**	**50**	**1**	**9**	**11**	**110**	**Both**	**61**
Sr	88	1	1	9	11	110	Both	12
Y	89	1	1	9	11	110	Both	12
Zr	90	1	1	9	11	110	Both	12
Nb	93	1	1	9	11	110	Both	12
Cs	**133**	**45**	**1**	**9**	**11**	**110**	**Both**	**56**
Ba	137	1	1	9	11	110	Both	12
La	139	1	1	9	11	110	Both	12
Ce	140	1	1	9	11	110	Both	12
Pr	141	1	1	9	11	110	Both	12
Nd	146	1	1	9	11	110	Both	12
Sm	149	1	1	9	11	110	Both	12
Eu	151	1	1	9	11	110	Both	12
Gd	157	1	1	9	11	110	Both	12
Tb	159	1	1	9	11	110	Both	12
Dy	163	1	1	9	11	110	Both	12
Ho	**165**	**30**	**1**	**9**	**11**	**110**	**Both**	**41**
Er	167	1	1	9	11	110	Both	12
Tm	169	1	1	9	11	110	Both	12
Yb	173	1	1	9	11	110	Both	12
Lu	175	1	1	9	11	110	Both	12
Hf	177	1	1	9	11	110	Both	12
Ta	181	1	1	9	11	110	Both	12
Pb	**208**	**37**	**1**	**9**	**11**	**110**	**Both**	**48**
Th	232	1	1	9	11	110	Both	12
U	238	1	1	9	11	110	Both	12

Elements shown in bold-face font correspond to magnet jumps.

on the selected masses. In order to achieve the most rapid acquisition of signals, we used the capability of the Element mass spectrometer to scan the mass spectrum in magnetic and electrostatic mode. Magnetic scanning requires settling times of about 1 ms/a.m.u. (atomic mass unit). The electrostatic scan allows rapid (1 ms of settling independent of the mass jump), quadrupole-style switching of peaks over up to 30% of the current "magnet mass", that is, the mass set by the magnet, by decreasing the accelerating voltage of the ions. Owing to the mass-range limitation of the electrostatic mode, six mass jumps ($^{25}Mg \rightarrow {}^{43}Ca \rightarrow {}^{85}Rb \rightarrow {}^{133}Cs \rightarrow {}^{165}Ho \rightarrow {}^{208}Pb$) were required for the acquisition of the selected masses. Settling times at each mass jump were roughly set by monitoring the stabilization of the voltage applied to the magnet as read on the field probe with an oscilloscope. Fine setting was performed with solution-nebulization by monitoring, on-line, the shape and the position of peaks within mass windows. The fly-back from ^{238}U to ^{25}Mg required the highest settling time (80 ms); the others vary between 30 and 50 ms as a function of the mass jump. Settling times for masses acquired in electrostatic scan mode were set to 1 ms. With the exception of ^{25}Mg and ^{29}Si, the best compromise between settling and counting time in peak acquisition was achieved with nine points per peak, a sample time of 1.0 ms, and an acquisition mass-window (*i.e.,* the mass range around the peak center that is acquired) of 110% of the peak width measured at 5% of the peak height. Because ^{25}Mg and ^{29}Si are the first masses acquired after the fly-back, larger mass-windows (160%) were set in order to compensate for the lower accuracy of the magnet during fast scanning. The choice of a lower number of samples per peak (3) for ^{25}Mg allowed a short duration of the segment. Peak intensity is obtained by averaging the intensities of the samples within a mass window ("integration window") of 100% of the peak width. For trace elements, signal detection was performed in "both" modes, that is, the signals were acquired in both ion counting and analog mode simultaneously. The two modes are automatically cross-calibrated by the software. Below 5 million counts per second, the reading from the counting mode is retained. Hence, where elements in both the external standard (*e.g.,* NIST 612) and the unknown sample are at trace level, as for the samples in this study, the acquisition of signals is in fact operated in counting mode. For major elements, the acquisition is set to "analog" mode.

TABLE 3. ACQUISITION PARAMETERS FOR U–Pb DETERMINATIONS IN ZIRCON

Element	Mass	Settling time (ms)	Sample time (ms)	Samples per peak	Mass window (%)	Segment duration (ms)
Hg	201	40	1.5	12	120	22
Pb	204	6	1.5	12	120	22
Pb	206	5	3.5/1.5	6/12	120	28/22
Pb	207	2	1.5	12	120	22
Pb	208	2	1.5	12	120	22
Th	232	25	3.5	6	120	28
U	235	6	1.5	12	120	22
U	238	6	3.5	6	120	28

Double values for ^{206}Pb correspond to its acquisition in analog and counting mode, respectively.

As reported in Table 2, the total scan-time of the 34 selected masses is about 700 ms, the settling time is about 340 ms, and hence the acquisition efficiency is estimated at about 50%. A typical analysis consists of acquiring one minute of background and one minute of ablated sample, thus approximately 170 sweeps are required. The mean integrated time for acquisition is about 0.9 s for each element. A typical analytical run consists of 20 analyses in which the first and last two are standard materials. Data reduction is performed by means of the GLITTER® software (Macquarie Research Ltd., 2001) developed by Van Achterbergh *et al.* (1999).

U–Pb dating of zircon

For the U–Pb dating of zircon, signals of masses ^{201}Hg, $^{204}(Pb+Hg)$, ^{206}Pb, ^{207}Pb, ^{208}Pb, ^{232}Th, ^{235}U and ^{238}U were acquired. The ^{201}Hg signal was collected in order to correct the isobaric interference of ^{204}Hg on ^{204}Pb (Horn *et al.* 2000).

The 201–238 mass range can be acquired both in magnetic and electrostatic mode because ^{238}U is about 16% heavier than ^{201}Hg, well within the 30% mass range allowed by the electrostatic scan. However, the electrostatic mode may introduce a further mass-discrimination owing to the decrease in sensitivity with increasing difference in masses from the nominal mass of the magnet (Fig. 1). We therefore preferred to acquire the selected masses in magnetic scan mode for the preliminary tests reported in this work. A settling time of <6 ms allows magnet stabilization for all masses with the exception of the fly-back from ^{238}U to ^{201}Hg and the mass jump from ^{208}Pb to ^{232}Th. These required 40 ms and 25 ms, respectively. Because of the generally high concentrations of Th and U in zircon and the high isotopic abundance, ^{238}U and ^{232}Th were detected in analog mode. In old U-rich crystals of zircon, analog detection of ^{206}Pb was also required. For signals acquired in counting mode, the best compromise in peak acquisition was achieved with 12 samples per peak, a sample time of 1.5 ms and a mass window of 120%. For masses acquired in analog mode, greater time per sample (3.5 ms) and fewer samples per peak (6) were used. This approach was required in order to decrease the offset signal of the analog detector, which is inversely proportional to the sampling time at short sampling times. Using the acquisition parameters displayed in Table 3, the total scan-time was approximately 290 ms, and the acquisition efficiency, about 63%.

U–Pb analyses of zircon consist of one minute of background and one minute of ablation signal, corresponding approximately to 410 sweeps and thus giving a mean integrated acquisition-time of 4 s for each element. Data reduction was performed with the software package LamTrace developed by S. Jackson, initially at Memorial University of Newfoundland and later at Macquarie University, Sydney. The analytical protocol included four standard analyses at the beginning and end of the analytical run.

Results on Element Concentrations

Response curve

In Figure 1, the response curves (*i.e.,* variation of sensitivity normalized to isotopic abundance relative to atomic mass units) determined using the conventional ICP-torch and the capacitive decoupling torch are reported. The data were obtained on the NIST 612 glass reference material using a 40 μm spot size, acquisition parameters listed in Table 2, He as a carrier gas, and a laser power of 2.2 mW at a frequency of 10 Hz. If only the masses acquired in a magnetic scan are considered (cross symbols), the increase in sensitivity with increasing mass unit is evident. The gain in sensitivity at each mass jump decreases toward higher masses, about 4–5 times from ^{25}Mg to ^{44}Ca, 1.5 times from ^{133}Cs to ^{165}Ho, and slightly negatively from ^{165}Ho to ^{208}Pb because the instrument was optimized for maximum sensitivity on ^{139}La and ^{232}Th. In the full mass-range considered, the overall increase in sensitivity approximates one order of magnitude. Sensitivity steadily decreases, for electrostatically set masses, with distance from the magnet mass. The loss in sensitivity is calculated to be 40% at the maximum mass allowed by the electrostatic scan-mode (*i.e.,* 30% of the nominal mass of the magnet). The effect of the electrostatic scan on sensitivity is clear in the response curve for the conventional torch, whereas much more scatter is observed in that for the capacitive decoupling torch. Nevertheless, in dry plasma conditions, the capacitive decoupling torch allows a four-fold increase in sensitivity relative to the conventional torch (Fig. 1), with average values at high masses of about 35000 cps/ppm under the conditions of the laser probe reported above.

Limits of detection

Limits of detection (DL) in LA–ICP–MS are a function of background signal, counting time per element and sensitivity, this latter in turn depending on the

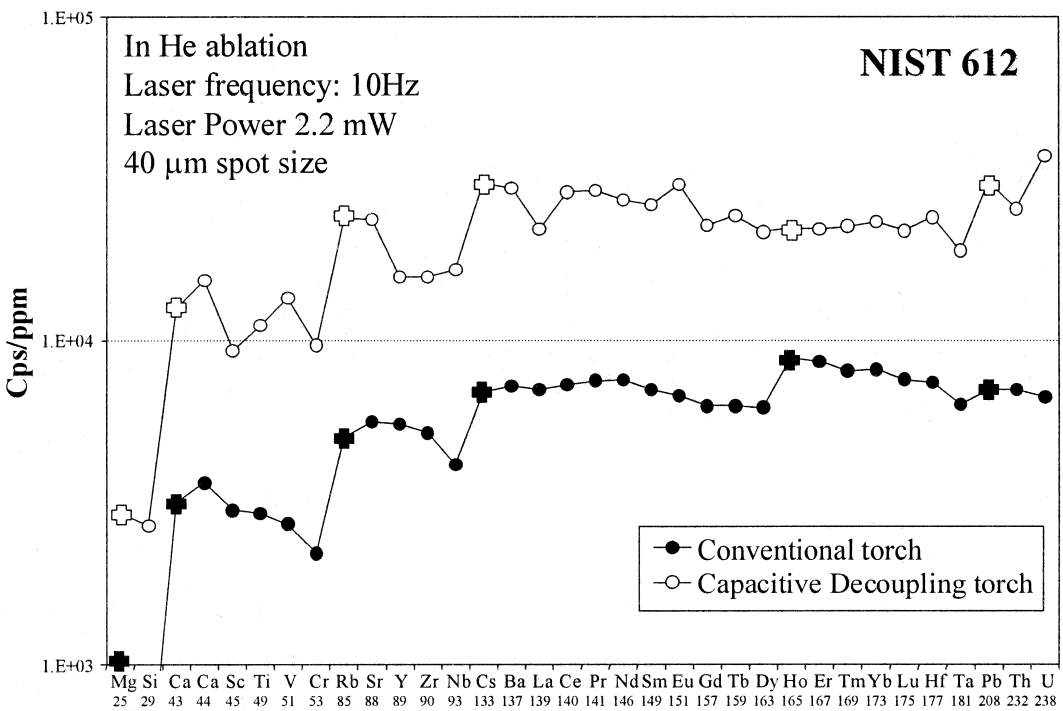

FIG. 1. Response curve. Cross symbols represent magnetic jumps.

amount of ablated material, *i.e.*, on spot size and laser power (Jackson *et al.* 1992), as well as isotopic abundance. Average minimum detection-limits (99% confidence, Longerich *et al.* 1996) of 34 selected elements (Table 4) were determined on the reference glass BCR–2 using the acquisition parameters of Table 2, He as carrier gas, and a laser frequency of 10 Hz. In order to constrain the variation of detection limits as a function of spot size, analyses were carried out at 40 and 15 μm spot size with a laser power of 1.0 and 0.3 mW, respectively. The limits of detection decrease (Fig. 2) with increasing mass, owing to their stringent relationship with sensitivity and background. At 40 μm spot size, the limits of detection are about 1 ppb for elements with high-abundance isotopes, and better than 10 ppb for the other elements. The higher-detection limits (10–100 ppb) quoted for ^{157}Gd and ^{208}Pb are related to the low isotopic abundance and the relatively high background, respectively. Masses lower than ^{139}La display limits of detection between 10 and 100 ppb. Exceptions are Y and Nb (<10 ppb), and Cr and Ti (between 0.1 and 1 ppm). By decreasing the pit size from 40 to 15 μm, the detection limits increase about three times without any significant fractionation among the various elements.

TABLE 4. MINIMUM LIMITS OF DETECTION (99% CONFIDENCE) ON THE USGS STANDARD BCR–2 BASALTIC GLASS

	40 μm	15 μm		40 μm	15 μm		40 μm	15 μm
Sc	0.118	0.421	Ba	0.024	0.100	Ho	0.001	0.002
Ti	0.654	1.802	La	0.002	0.007	Er	0.003	0.016
V	0.019	0.069	Ce	0.002	0.008	Tm	0.001	0.003
Cr	0.412	1.553	Pr	0.001	0.004	Yb	0.004	0.013
Rb	0.045	0.158	Nd	0.004	0.019	Lu	0.001	0.003
Sr	0.015	0.055	Sm	0.006	0.017	Hf	0.005	0.018
Y	0.005	0.017	Eu	0.002	0.009	Ta	0.002	0.006
Zr	0.059	0.206	Gd	0.015	0.061	Pb	0.015	0.055
Nb	0.003	0.011	Tb	0.001	0.004	Th	0.001	0.003
Cs	0.022	0.075	Dy	0.004	0.013	U	0.001	0.002

Concentrations are quoted in ppm.

Precision and accuracy

As for limits of detection, precision is also a function of the total number of ions of analyte detected (Günther *et al.* 1995). Therefore, it depends, leaving the acquisition parameters constant, on the analyte concentration and pit size. Precision and accuracy of our LA–ICP–MS were evaluated using two USGS basaltic glass

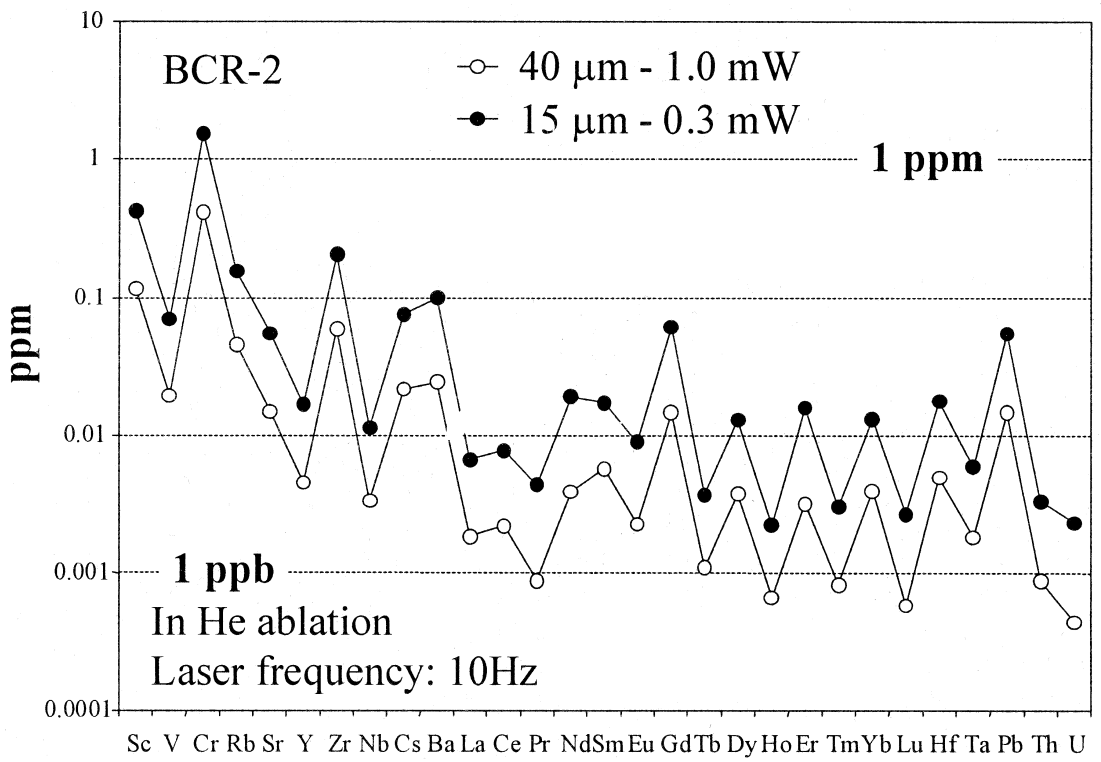

FIG. 2. Limits of detection of selected trace elements at different spot-sizes.

reference materials with different concentrations of trace elements: the Columbia River Basalt (BCR–2) and the Icelandic Basalt (BIR–1). Standard BIR–1 is significantly depleted (by more than one order of magnitude) in *LREE* (0.6–2.5 ppm), Nb (0.6 ppm), Ba (7 ppm) and Zr (18 ppm), when compared to BCR–2. Reference values for BCR–2 (Table 5) are those reported by the USGS (http://minerals.cr.usgs.gov/geochem/basaltbcr2.html) with the exception of Nb, Ta, Dy and Er (S. Jackson, pers. commun.). Reference values for BIR–1 are taken from Govindaraju (1994).

Precision is given at one relative standard deviation (RSD) and has been calculated on the basis of 14 replicates in one day. Analyses on both samples were carried out using 40 μm pit sizes, with He as a carrier gas, a laser frequency of 10 Hz, and a laser power of 1.0 mW. Trace-element concentrations were quantified using the NIST 612 glass as an external standard and ^{44}Ca as an internal standard. Average values are reported in Table 5 and shown in Figure 3. A precision better than 7% was found for all elements in BCR–2. Owing to the lower concentration of analyte, a slightly lower precision was achieved on BIR–1. Values are generally better than 10%, with the exception of Rb, Ta, Th and U, owing to their very low concentrations.

Accuracy, given as the relative difference from reference values, is reported in Table 5. As shown in Figure 4, accuracy for the BCR–2 reference glass is always better than 11%, with most elements in the range ±5%. Accuracy values agree to better than 20% on the BIR–1 reference glass, with the exception of Cr, Pb and U. The low accuracy obtained on U is likely related to its great dilution (10 ppb) in this sample.

Comparison with the quadrupole-based LA–ICP–MS approach

A direct comparison of our results with those obtained with quadrupole-based LA–ICP–MS is not straightforward because of the strong influence of the ablation conditions (*e.g.,* spot diameter and laser energy). Nevertheless, some qualitative considerations may be based on data reported in literature. Limits of detection of our instrument, if compared with those obtained with a standard quadrupole-based instrument at similar conditions of ablation (40 μm; Günther *et al.* 2000), are significantly lower (approximately one order of magnitude) in the high-mass range, and comparable in the low-mass range. At high masses, our limits of detection are still generally better (1.5–2 times) than

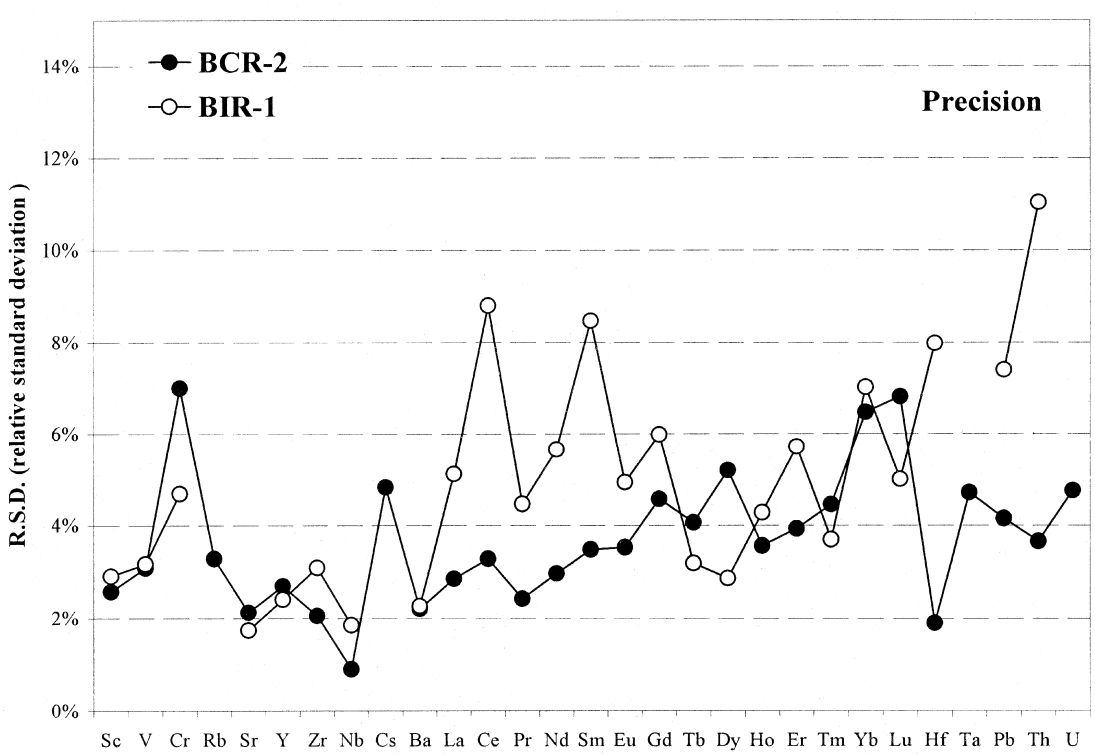

FIG. 3. Precision at 1σ (%) obtained on the two USGS reference materials BCR–2 and BIR–1.

those obtained by Günther *et al.* (1996) with a quadrupole used with a modified sampler orifice. Nevertheless, at lower masses (<93 a.m.u.), despite the higher sensitivity of our instrument, the higher background signal causes slightly higher limits of detection. The average precision and accuracy are comparable to those obtained with quadrupoles (Günther *et al.* 1995, Longerich *et al.* 1996), and slightly better precision than Norman *et al.* (1996) achieved on the USGS reference basaltic glass BIR–1.

These results show that in terms of overall performance for trace element determinations, our laser probe coupled with a sector-field mass spectrometer can compete with the quadrupole-based instruments so far adopted by most laboratories. The major requirements for a mass spectrometer to be used in conjunction with a LA sampler, *i.e.*, rapid scanning, high sensitivity and low background, are all fulfilled. The instrumental setup pursued in our laboratory, along with the proper analytical protocol, allows quantitative microanalysis for trace elements to be carried out on a routine basis.

TABLE 5. PRECISION AND ACCURACY DETERMINED ON BCR-2 AND BIR-1, USGS REFERENCE MATERIALS

	BCR-2					BIR-1				
	Ref. values	Meas. values (n = 14)	Stdev (1σ)	RSD %	Accuracy %	Ref. values	Meas. values (n = 14)	Stdev (1σ)	RSD %	Accuracy %
Sc	33	34.7	0.9	2.6	4.9	44	40.51	1.18	2.9	-8.6
V	416	451	13.9	3.1	7.7	313	370	11.79	3.2	16
Cr	18	18.4	1.3	7.0	2.3	382	507	23.73	4.7	25
Rb	48.0	51.3	1.7	3.3	6.4	0.25	0.21	0.09	41	-17
Sr	346	352	7.5	2.1	1.8	108	118	2.06	1.7	8.7
Y	37.0	34.3	0.9	2.7	-7.8	16	13.8	0.33	2.4	-16
Zr	188	197	4.1	2.1	4.8	15.5	14.7	0.46	3.1	-5.1
Nb	13.1*	14.8	0.1	0.9	11	0.6	0.65	0.01	1.9	7.9
Cs	1.1	1.1	0.1	4.8	-0.6	---	---	---	---	---
Ba	683	717	15.9	2.2	4.7	7	7.01	0.16	2.3	0.1
La	25	25.1	0.7	2.9	0.5	0.62	0.60	0.03	5.1	-2.7
Ce	53.0	56.1	1.8	3.3	5.5	1.95	2.20	0.19	8.8	11
Pr	6.8	7.0	0.2	2.4	3.4	0.38	0.39	0.02	4.5	3.1
Nd	28.0	29.6	0.9	3.0	5.3	2.5	2.54	0.14	5.7	1.4
Sm	6.7	6.7	0.2	3.5	-0.1	1.1	1.13	0.10	8.5	3.0
Eu	2	2.1	0.1	3.5	4.3	0.54	0.57	0.03	4.9	4.5
Gd	6.8	6.3	0.3	4.6	-7.8	1.85	1.61	0.10	6.0	-15
Tb	1.07	1.0	0.0	4.1	-8.2	0.36	0.32	0.01	3.2	-12
Dy	6.38*	6.3	0.3	5.2	-1.2	2.5	2.49	0.07	2.9	-0.5
Ho	1.33	1.3	0.0	3.6	-5.9	0.57	0.56	0.02	4.3	-2.0
Er	3.66*	3.6	0.1	3.9	-0.7	1.7	1.68	0.10	5.7	-1.2
Tm	0.54	0.5	0.0	4.5	-11	0.26	0.24	0.01	3.7	-9.4
Yb	3.5	3.4	0.2	6.5	-2.0	1.65	1.72	0.12	7.0	4.2
Lu	0.51	0.5	0.0	6.8	-8.5	0.26	0.24	0.01	5.0	-9.1
Hf	4.8	4.8	0.1	1.9	0.6	0.6	0.59	0.05	8.0	-1.4
Ta	0.78*	0.8	0.0	4.7	4.0	0.04	0.04	0.01	19	10
Pb	11.0	11.5	0.5	4.2	4.5	3	4.12	0.30	7.4	27
Th	6.2	6.2	0.2	3.7	0.05	0.03	0.029	0.003	11	-2.5
U	1.69	1.9	0.1	4.8	8.6	0.01	0.018	0.004	23	44

Reference values for BCR-2 are taken from the USGS web site: (http://minerals.cr.usgs.gov/geochem/basaltbcr2.html), with the exception of elements marked with * (S.E. Jackson, pers. commun.). Reference values for BIR-1 are from Govindaraju (1994). Concentrations are expressed in ppm.

Results on U–Pb Dating of Zircon

One of the major impediments in dating zircon crystals by means of LA–ICP–MS is the elemental fractionation induced by ablation, transport and excitation processes (Longerich *et al.* 1996b, Jackson 2001, Günther & Hattendorf 2001), which alters the original values of the isotope ratios. Elements most affected by fractionation are those with differential volatilities, such as U and Pb (Fryer *et al.* 1993, Longerich *et al.* 1996b, Hirata 1997), on which the geochronology of zircon is based. Major efforts in reducing the U–Pb fractionation during the ablation process were made by controlling laser-focusing conditions, crater aspect-ratio, density of laser energy and temperature distribution. Stable signals and reduced fractionation of elements are achieved by focusing the laser above the sample surface, thus minimizing its defocusing with ablation depth (Jackson 2001). U–Pb fractionation is also strongly reduced if one uses large pits of shallow depth (Eggins *et al.* 1998, Mank & Mason 1999, Horn *et al.* 2000) or adopts the "cooling-jet cell" (Jackson *et al.* 1996), and uses He as a carrier gas (Eggins *et al.* 1998, Günther & Heinrich 1999) in order to reduce the thermal gradient at the ablation site. Good results on U–Pb fractionation come from the adoption of laser sources with a highly homogeneous density of energy, such as 193 nm excimer lasers (Horn *et al.* 2000) or the recently homogenized 266 nm Nd:YAG laser (Horn & Günther 2001, Guillong *et al.* 2002). To reduce U–Pb fractionation, many researchers (*e.g.*, Li *et al.* 2001, Horstwood *et al.* 2001) are currently adopting the "rastering" method, which consists of mechanically displacing the laser beam on the sample surface in order to prevent the formation of deep craters. Although very effective, we contend that this method places a strong limitation on the spatial resolution of the technique, an aspect that is extremely important, especially in zircon with inherited components.

Evaluation of the fractionation of U and Pb

In order to evaluate the fractionation of U and Pb with our instrument, tests were performed with He as the carrier gas, with the laser focused above the sample on two well-characterized samples of zircon: zircon standard 91500 (Wiedenbeck *et al.* 1995) and zircon 02123 (TIMS data by Ketchum *et al.* 2001). The fragments of zircon were mounted in epoxy resin and then polished and washed in an ultrasonic bath in order to remove surface contamination. Analyses were carried out at different spot-size (20, 40, 60, 80 μm) at a constant density of energy of 18 J/cm^2, laser frequency of 10 Hz and with acquisition parameters shown in Table 3. The fractionation of U and Pb was evaluated on a relative basis by considering the slope of the regression line of $^{206}Pb/^{238}U$ *versus* time calculated in an interval of 60 s and normalized to the average value. The fractionation slope thus obtained is the relative variation of

the $^{206}Pb/^{238}U$ value per second. These values multiplied by 60 and 100 show the percent variation per minute, the average duration of a typical analysis.

The average values of fractionation slope for different runs at different spot-size, calculated averaging results of eight analyses for each fragment of zircon, are reported in Figure 5a. The laser-induced $^{206}Pb/^{238}U$ fractionation decreases from a maximum of 17% at 20 μm spot to a minimum of 3% at 80 μm spot. The average values of fractionation slope for each fragment of zircon at the same spot-size are reported in Table 6, and in Figure 5b they are compared with the calibration curve obtained by Horn *et al.* (2000) with an excimer laser at 193 nm. The trend obtained in this study closely resembles that of Horn *et al.* (2000), but is roughly twice as high.

Strategies for the correction of the fractionation of U and Pb include the adoption of matrix-matched standards or the complete mathematical parameterization of the U/Pb dependences on spot geometry (Horn *et al.* 2000). The former requires the constancy of density of energy, spot size, repetition rate and integration time between unknown sample and external standard, whereas with the latter, only the density of energy has to remain constant because all the other parameters are required as input of the empirical calibration equation (Horn *et al.* 2000). This calibration needs a high reproducibility of the elemental fractionation at constant density of energy. However, the preliminary data with our system show that the reproducibility of the fractionation slope at the same pit-size in runs carried out on different days is poor. If we consider the run carried out at a 40-μm spot, day-to-day variability of the laser homogeneity induces a variation of the daily average fractionation slope up to 20% relative for zircon 02123 and up to 60% relative for zircon 91500. This pattern prevents us from applying a mathematical correction as that of Horn *et al.* (2000).

At present, we thus have to rely on the external standard calibration procedure, which requires a good reproducibility of the fractionation within a run and among different samples. The intra-run difference in the average variation of the fractionation of U and Pb over 1 minute between zircon samples 02123 and 91500 goes from –1.8 to 3.6%, with an average of 0.2%. This is the range of the residual error stemming from elemental fractionation that would not be corrected when using one zircon sample to calibrate the second.

However, these results are not directly exportable to other zircon samples because of the similar optical and

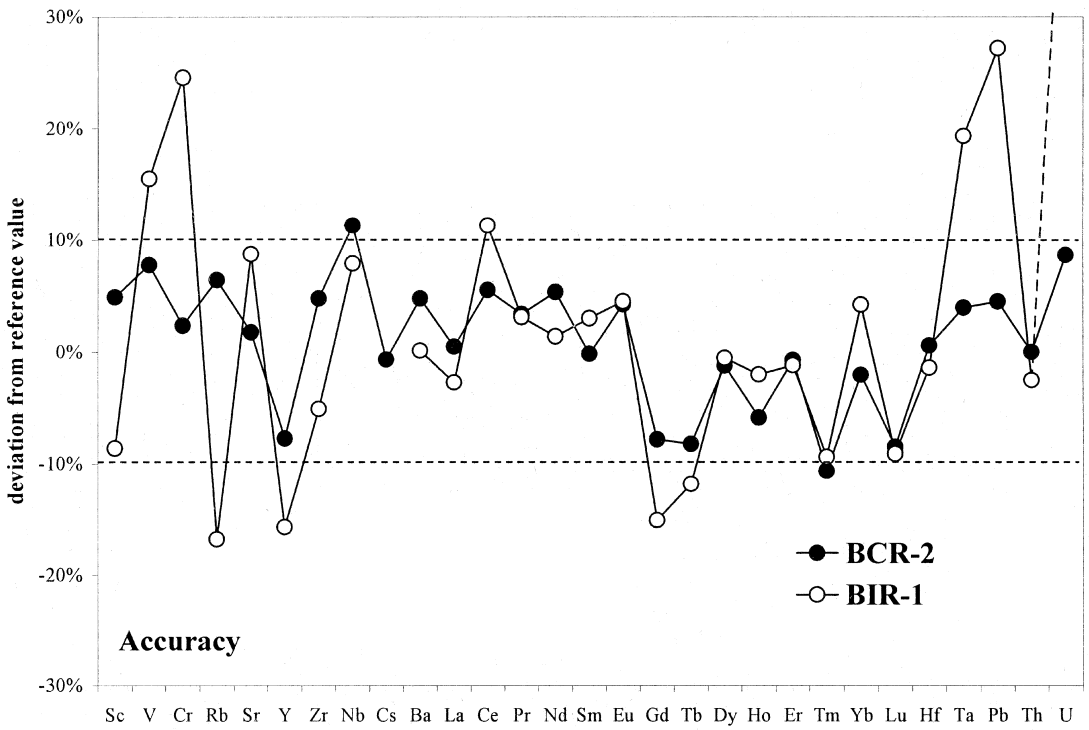

FIG. 4. Accuracy at 1σ (%) obtained on the two USGS reference materials BCR–2 and BIR–1.

cathodoluminescence (CL) properties of the two samples of zircon used in this study, factors that may influence the ablation process. Analyses were thus carried out at the maximum spot-size (40 μm) allowed by the grain dimensions of two other samples of zircon with different ages (GRM: 350 Ma and GRP: 500 Ma) and different CL emissions. A peculiar feature of zircon GRM is also a marked oscillatory zoning of trace elements. In order to better control the agreement between standard and unknown, these analyses were performed as independent analytical runs consisting of eight determinations of the unknown between two groups of four determinations of the standard. Zircon GRM was standardized with zircon 02123, and zircon GRP, with zircon 91500. The average difference in the variation of the Pb/U value in a 60-second integration interval be-

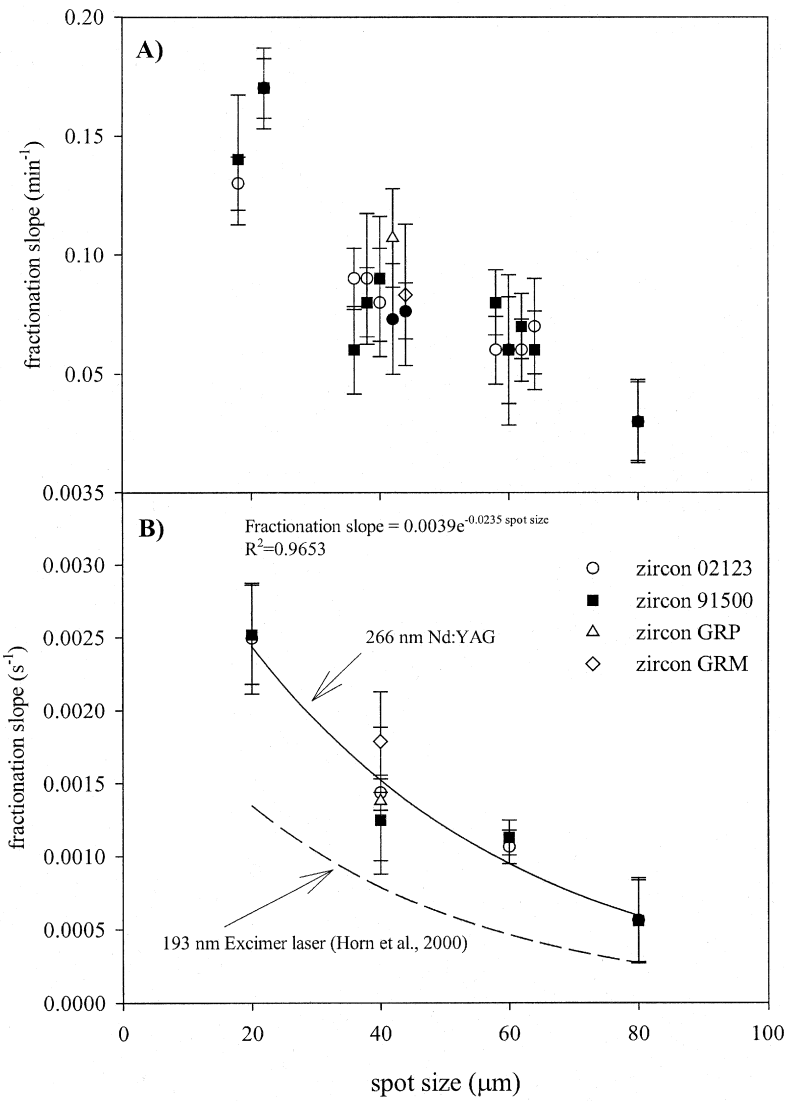

FIG. 5. A) Variation of the average U/Pb fractionation (min^{-1}) as a function of the spot size for each analytical run. B) Variation of the U/Pb fractionation slope (s^{-1}), obtained averaging all data carried out at the same spot-size, as a function of the spot size. For comparison, the experimental curve obtained with a 193 nm excimer laser by Horn *et al.* (2000) is reported. Error bars represent 1 σ.

tween the standard and the unknown is better than 0.7% for zircon GRP and 3.5% for zircon GRM, within the range obtained on the two standard samples of zircon in previous runs.

Even if the error from differences in fractionation certainly contributes to the final accuracy of the $^{206}Pb/^{238}U$ value, we did not find any evident correlation, and we must conclude that other sources of error are predominant at this stage. For GRM zircon, for example, the instability of the signal points to possible error arising from zonation or fractures.

Determination of values of isotope ratios

The capability of our instrument to produce reliable U–Pb ages was tested on zircon 91500 (1062.4 Ma; Wiedenbeck *et al.* 1995) using zircon 02123 (295 Ma; Ketchum *et al.* 2001) as the external standard. In each analytical run, the same spot-size, density of energy and rate of repetition were used for external standard and unknown sample (zircon 91500). Data reduction was performed by means of the software package LAMTRACE; we adopted the same integration intervals (1 minute for background and 1 minute for signal) on every replicate. ICP–MS capabilities (*i.e.*, high sensitivity to abundance and low background) and the adoption of external standards allowed the determination of the $^{207}Pb/^{235}U$ value, which is usually extrapolated from $^{206}Pb/^{238}U$ using quadrupole-based instruments and internal standardization for mass-bias correction (*e.g.*, Horn *et al.* 2000). In Table 7, values of the isotope ratios $^{206}Pb/^{238}U$, $^{207}Pb/^{235}U$, $^{207}Pb/^{206}Pb$ and $^{208}Pb/^{232}Th$ and relative standard deviations are reported for zircon 91500. Data were corrected using the data block obtained for the external standard at the same spot-size. No correction for common lead was applied, because ^{204}Pb is within the background signal after the subtraction of ^{204}Hg interference on mass 204.

The average of replicates for $^{206}Pb/^{238}U$ and $^{207}Pb/^{235}U$ on zircon 91500 agrees with the TIMS values (Wiedenbeck *et al.* 1995) within 2% for 40- and 60-μm spot-sizes. For 20- and 80-μm spots, accuracy is slight lower (–3.3 to 2.7%). For pit sizes of 40 μm or larger, the relative standard deviations (1σ) of the mean of each individual analysis to which the uncertainty on the age calculation is related, is about 0.56–1.14% for $^{206}Pb/^{238}U$, 0.74–1.46% for $^{207}Pb/^{235}U$ and 0.56–1.16% for $^{207}Pb/^{206}Pb$. Slightly higher RSD ($^{206}Pb/^{238}U < 1.5\%$, $^{207}Pb/^{235}U < 2.7\%$, $^{207}Pb/^{206}Pb < 2.8\%$) were achieved with a 20-μm spot. Such standard deviations allow us to obtain zircon ages that are still geologically meaningful. RSD values are comparable to those of Horn *et al.* (2000) obtained with an excimer laser, which produces more homogeneous ablation relative to our 266 nm Nd:YAG. As for old crystals of zircon (>500 Ma), values of the RSD also favorably compare with those obtained by SHRIMP (Williams 1998). As shown by current and literature data, the precision given by micro-analytical techniques is significantly lower relative to that attained with bulk analysis (TIMS). Nevertheless, this is counterbalanced by the larger amount of information that the high spatial resolution can allow on zoned crystals of zircon. Reproducibility (relative standard deviation of the average ratio) is estimated better than 4.3% for the three isotope ratios at a spot size ≥ 40 μm. $^{206}Pb/^{238}U$ and $^{207}Pb/^{235}U$ ages are reported in Table 8 together with 2σ absolute standard deviation and plotted in the concordia diagram in Figure 6. The weighted average of $^{206}Pb/^{238}U$ ages on all replicates at various spot-sizes is 1054 ± 10 Ma (2σ), the $^{207}Pb/^{206}Pb$ age is 1057 ± 11 Ma (n = 31), both close to the TIMS values of 1065.4± 0.3 Ma and 1062.4 ± 0.8 Ma, respectively.

TABLE 6. RESULTS ON LASER-INDUCED FRACTIONATION OF ELEMENTS

	Spot size (μm)	$^{206}Pb/^{238}U$ fractionation s^{-1}	1 σ	$^{206}Pb/^{238}U$ fractionation min^{-1}
Zircon 02123				
Fe07b	20	0.22%	0.02%	13%
Fe13a	20	0.28%	0.03%	17%
Fe06b	40	0.16%	0.02%	9%
Fe13b	40	0.15%	0.05%	9%
Fe21a	40	0.13%	0.04%	8%
Fe06c	60	0.10%	0.02%	6%
Fe13c	60	0.10%	0.05%	6%
Ma08a	60	0.10%	0.02%	6%
Ma09a	60	0.12%	0.03%	7%
Fe07a	80	0.06%	0.03%	3%
Ap18a	40	0.12%	0.04%	7%
Zircon 91500				
Fe07b	20	0.23%	0.05%	14%
Fe13a	20	0.28%	0.02%	17%
Fe06b	40	0.10%	0.03%	6%
Fe13b	40	0.13%	0.02%	8%
Fe21a	40	0.15%	0.04%	9%
Fe06c	60	0.13%	0.02%	8%
Fe13c	60	0.10%	0.04%	6%
Ma08a	60	0.11%	0.02%	7%
Ma09a	60	0.11%	0.03%	6%
Fe07a	80	0.06%	0.03%	3%
My08a	40	0.13%	0.02%	8%
Samples of natural zircon that are not standards				
Ap18a(GRM)	40	0.18%	0.03%	11%
My08a(GRP)	40	0.14%	0.05%	8%
Intra-run agreement				
Fe07b	20	---	---	–0.3%
Fe13a	20	---	---	0.0%
Fe06b	40	---	---	3.6%
Fe13b	40	---	---	1.0%
Fe21a	40	---	---	–1.2%
Fe06c	60	---	---	–1.8%
Fe13c	60	---	---	–0.2%
Ma08a	60	---	---	–0.4%
Ma09a	60	---	---	1.0%
Fe07a	80	---	---	0.0%
Ap18a(GRM)	40	---	---	–3.4%
My08a(GRP)	40	---	---	–0.7%

We are currently evaluating whether the signal acquisition in electrostatic mode is more convenient than in magnetic mode. An electrostatic scan is significantly faster and allows higher efficiency in acquisition (~90%); thus, a gain in precision and detection limits is to be expected. The tests are aimed to assess whether the loss in sensitivity that occurs for masses far from the magnet mass can reduce or even nullify this gain. Another purpose of the tests is the evaluation of the youngest detectable age; the first analyses performed on a young zircon (TIMS $^{207}Pb/^{206}Pb$ age of 150 ± 2 Ma with about 1 ppm of Pb; Jean-Louis Paquette, pers. commun.) are encouraging. Preliminary results show that despite the very low concentrations of Pb, the relative standard deviation on the ratio $^{206}Pb/^{238}U$ is low (~2.0%), and the accuracy on the ages is better than 3%.

TABLE 7. VALUES OF ISOTOPE RATIOS FOR ZIRCON 91500 AND 1σ RELATIVE STANDARD DEVIATIONS

spot size	$^{206}Pb/^{238}U$ value	1σ	$^{207}Pb/^{235}U$ value	1σ	$^{207}Pb/^{206}Pb$ value	1σ	$^{208}Pb/^{232}Th$ value	1σ
20 μm	0.185	1.30	1.86	2.55	0.0730	2.49	0.0525	2.29
20	0.172	1.36	1.73	2.23	0.0730	2.24	0.0512	2.14
20	0.181	1.47	1.76	2.65	0.0705	2.73	0.0482	2.74
20	0.181	1.17	2.00	2.02	0.0798	1.91	0.0560	1.92
20	0.177	1.32	1.79	2.42	0.0731	1.96	0.0530	2.09
20	*0.190	*5.59	*1.801	*2.49	*0.0687	*2.66	*0.0510	*2.15
20	0.174	1.38	1.80	2.41	0.0752	2.35	0.0521	2.12
20	0.176	1.23	1.90	2.59	0.0782	2.43	0.0555	2.11
mean	**0.178**	**2.60**	**1.834**	**5.00**	**0.0747**	**4.40**	**0.0526**	**5.02**
% deviation from reference	–0.66		–0.90		–0.27		–2.11	
40 μm	0.170	1.00	1.79	1.41	0.0765	1.16	0.0523	0.99
40	0.167	0.99	1.72	1.11	0.0746	1.11	0.0488	0.97
40	0.170	0.94	1.79	1.21	0.0766	1.09	0.0515	1.01
40	0.189	0.93	1.96	1.37	0.0751	0.99	0.0514	1.05
40	0.180	1.00	1.93	1.33	0.0776	1.05	0.0500	0.83
40	0.182	1.14	1.89	1.46	0.0752	1.17	0.0515	0.82
40	0.175	1.08	1.84	1.34	0.0763	0.92	0.0500	0.79
40	0.181	0.91	1.89	1.27	0.0759	1.00	0.0501	0.90
mean	**0.177**	**4.25**	**1.851**	**4.29**	**0.0760**	**1.28**	**0.0507**	**2.27**
% deviation from reference	–1.46		0.03		1.43		–6.02	
60 μm	0.183	0.61	1.88	0.75	0.0744	0.78	0.0482	0.58
60	0.174	0.65	1.79	0.74	0.0747	0.66	0.0477	0.69
60	0.178	0.63	1.83	0.77	0.0746	0.66	0.0500	0.61
60	0.178	0.65	1.85	0.77	0.0755	0.68	0.0486	0.60
60	0.174	0.68	1.79	0.89	0.0747	0.70	0.0492	0.72
60	0.176	0.69	1.83	0.76	0.0752	0.64	0.0504	0.70
60	0.175	0.56	1.78	0.72	0.0739	0.66	0.0507	0.56
60	0.174	0.60	1.77	0.76	0.0735	0.56	0.0521	0.63
mean	**0.176**	**1.80**	**1.814**	**2.14**	**0.0746**	**0.89**	**0.0496**	**2.96**
% deviation from reference	–1.54		–1.99		–0.43		–8.34	
80 μm	0.193	1.10	1.99	1.28	0.0748	0.77	0.0534	0.90
80	0.182	0.84	1.87	0.94	0.0747	0.72	0.0534	0.96
80	0.187	1.07	1.94	1.16	0.0751	0.91	0.0517	0.84
80	0.183	0.99	1.85	1.02	0.0737	0.73	0.0500	0.88
80	0.182	0.72	1.87	0.93	0.0743	0.78	0.0515	0.92
80	0.182	0.97	1.84	1.11	0.0731	0.84	0.0489	0.99
80	0.176	1.05	1.77	1.18	0.0731	0.84	0.0486	1.18
80	0.187	1.06	1.88	1.08	0.0727	0.80	0.0498	1.21
mean	**0.184**	**2.77**	**1.877**	**3.51**	**0.0739**	**1.24**	**0.0509**	**3.69**
% deviation from reference	2.72		1.45		–1.27		–5.55	
mean of all replicates	0.1788	3.37	1.8444	3.87	0.0748	2.41	0.0509	4.02
reference values	0.1792		1.8502		0.07488		0.05374	
% deviation from reference	–0.20		–0.32		–0.12		–5.57	

* rejected in the calculation of the mean owing to the high standard deviations. Standard deviation is expressed in %.

TABLE 8. AGES FOR ZIRCON 91500

spot size	$^{206}Pb/^{238}U$ age	2σ	$^{207}Pb/^{235}U$ age	2σ	$^{207}Pb/^{206}Pb$ age	2σ	$^{208}Pb/^{232}Th$ age	2σ
20 μm	1095	26	1068	34	1012	100	1034	46
20	1024	26	1021	29	1012	92	1009	42
20	1071	29	1030	34	942	112	951	51
20	1074	23	1114	27	1192	74	1100	41
20	1052	26	1041	31	1014	80	1045	43
20	*1121	*115	*1046	*33	*888	*110	*1005	*42
20	1032	26	1046	31	1072	96	1026	43
20	1044	24	1080	34	1150	96	1092	45
weighted mean	**1056**	**23**	**1059**	**32**	**1069**	**83**	**1041**	**45**
40 μm	1010	19	1042	18	1108	46	1030	20
40	997	18	1016	14	1056	44	962	18
40	1010	17	1042	16	1108	44	1014	20
40	1115	19	1101	18	1070	40	1012	21
40	1068	20	1091	18	1136	42	986	16
40	1078	23	1076	19	1072	48	1015	16
40	1039	21	1060	18	1102	36	986	15
40	1070	18	1078	17	1092	40	989	17
weighted mean	**1046**	**35**	**1059**	**25**	**1094**	**21**	**997**	**18**
60 μm	1084	12	1073	10	1050	32	951	11
60	1035	12	1043	10	1060	26	941	13
60	1054	12	1056	10	1058	28	986	12
60	1055	13	1064	10	1082	26	960	11
60	1032	13	1041	12	1058	28	970	14
60	1046	13	1056	10	1074	26	994	14
60	1038	11	1038	9	1038	26	1000	11
60	1036	12	1033	10	1026	24	1026	13
weighted mean	**1047**	**14**	**1050**	**12**	**1055**	**16**	**977**	**23**
80 μm	1140	23	1068	34	1062	32	1051	18
80	1077	17	1021	29	1060	30	1051	20
80	1107	22	1030	34	1070	36	1019	17
80	1081	20	1114	27	1030	30	987	17
80	1080	14	1041	31	1050	32	1015	18
80	1080	19	1046	33	1016	34	965	19
80	1046	20	1046	31	1016	34	959	22
80	1106	22	1080	34	1004	34	983	23
weighted mean	**1086**	**21**	**1057**	**27**	**1039**	**20**	**1006**	**29**
weighted mean	1054	10	1052	7	1057	11	989	11
reference values	1065.4	0.6	---	---	1062.4	0.8	1058.1	5.6
% deviation from reference	-1.1%	---	---	---	-0.5%	---	-7.0%	---

* rejected in the calculation of the mean owing to the high standard deviations.

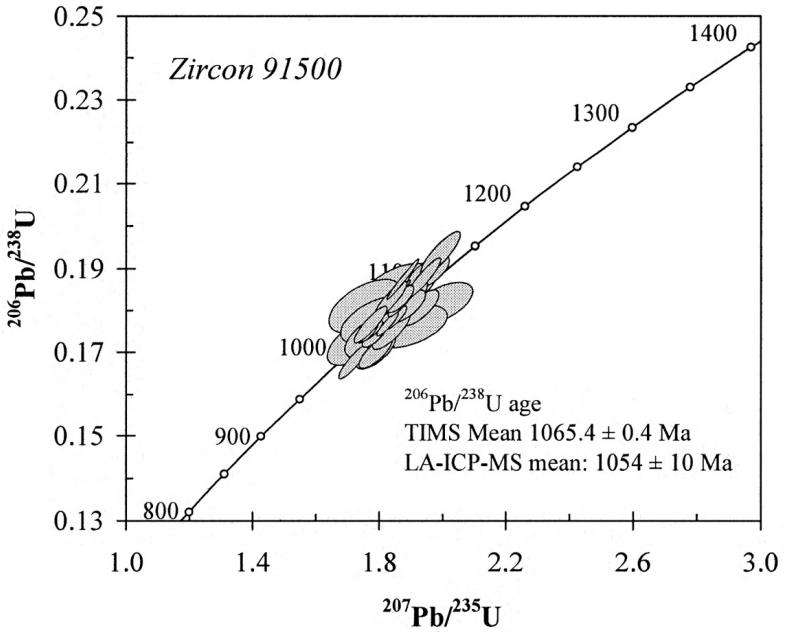

FIG. 6. Concordia diagram for zircon 91500. The diagram was made with "Isoplot/Ex" version 2.33 by K. Ludwig, Berkeley Geochronology Center.

The ratio $^{207}Pb/^{235}U$ is still detectable, even though with a high relative standard deviation (about 14%).

CONCLUSIONS

Sector-field mass spectrometers, so far considered too slow for the purpose, are suitable for the acquisition of the rapidly varying signals produced by laser ablation. The "Element" sector-field mass spectrometer, coupled with a 266 nm laser source, allows trace-element determination on geological samples to a good precision and accuracy (generally better than 10%). Thanks to the high sensitivity and low background, limits of detection are extremely low (down to the ppb level) for the heaviest elements. The first results on determinations of U–Pb ratios are also very positive, comparing well with the results found in the literature from other laboratories and other micro-analytical techniques (ion microprobes). Adopting an external matrix-matched standard for corrections of mass bias and laser-induced elemental fractionation, age precision and accuracy are attained to better than ~2% on a crystal of zircon with about 80 ppm of U.

ACKNOWLEDGEMENTS

We are indebted to Henry Longerich, Simon Jackson, Detlef Günther and Ingo Horn for helping us to understand several important aspects on the LA–ICP–MS technique at the time we were setting up the laboratory. Simon Jackson is also gratefully acknowledged for the many theoretical and practical advices he gave us. Detlef Günther and Ingo Horn on several occasions since then provided information and advice, which enabled us to significantly improve the LA–ICP–MS system in operation at CNR–CSCC, Pavia. Luisa Ottolini is thanked for her contribution at the start of the LA–ICP–MS project. Jean-Louis Paquette kindly provided zircon samples (GRP, GRM) and the reference age, determined by TIMS. The paper has benefitted from constructive reviews of I. Horn and M.S.A. Horstwood. Funding for this work was provided by Consiglio Nazionale delle Ricerche – Agenzia 2000 (project "Sviluppo di datazioni U/Pb di zirconi mediante Laser Ablation Microprobe – Inductively Coupled Plasma – Mass Spectrometry: prime applicazioni alla geocronologia di eventi magmatici connessi all'orogenesi Alpina") to Massimo Tiepolo. The P.N.R.A. has funded the purchase of the laser probe and the mass spectrometer.

REFERENCES

EGGINS, S.M., KINSLEY, L.P.J. & SHELLEY J.M.G. (1998): Deposition and elemental fractionation processes during atmospheric pressure laser sampling for analysis by ICP–MS. *Appl. Surf. Sci.* **127**, 278-286.

FRYER, B.J., JACKSON, S.E. & LONGERICH, H.P. (1993): The application of laser ablation microprobe – inductively coupled plasma – mass spectrometry (LAM–ICP–MS) to in situ (U)–Pb geochronology. *Chem. Geol.* **109**, 1-8.

GOVINDARAJU, K. (1994): 1994 compilation of working values and sample description for 383 geostandards. *Geostandards Newsletter* **18**, 1-158.

GUILLONG, M., HORN, I. & GÜNTHER, D. (2002): Capabilities of a homogenized 266 nm Nd:YAG laser ablation system for LA–ICP–MS. *J. Anal. At. Spectrom.* **17**, 8-14.

GÜNTHER, D. & HATTENDORF, B. (2001): Elemental fractionation in LA–ICP–MS. *In* Laser-Ablation-ICPMS in the Earth Sciences: Principles and Applications (P. Sylvester, ed.). *Mineral. Assoc. Can., Short Course* **29**, 83-93.

_____ & HEINRICH, C.A. (1999): Comparison of the ablation behavior of 266 nm Nd:YAG and 193 nm ArF excimer lasers for LA–ICP–MS analysis. *J. Anal. At. Spectrom.* **14**, 1369-1374.

_____, HORN, I. & HATTENDORF, B. (2000): Recent trends and developments in laser ablation – ICP – mass spectrometry. *Fresenius J. Anal. Chem.* **368**, 4-14.

_____, LONGERICH, H.P., FORSYTHE, L. & JACKSON, S.E. (1995): Laser ablation microprobe – inductively coupled plasma – mass spectrometry. *American Laboratory* **27**(9), 24-29.

_____, _____, JACKSON, S.E. & FORSYTHE, L. (1996): Effect of sampler orifice diameter on dry plasma inductively coupled plasma mass spectrometry (ICP–MS) backgrounds, sensitivities, and limits of detection using laser ablation sample introduction. *Fresenius J. Anal. Chem.* **355**, 771-773.

HIRATA, T. (1997): Soft ablation technique for laser ablation – inductively coupled plasma mass spectrometry. *J. Anal. At. Spectrom.* **12**, 1337-1342.

HORN, I. & GÜNTHER, D. (2001): 266 nm Nd:YAG ablation system? Strategies to influence the ablation characteristics. *Geol. Assoc. Can. – Mineral. Assoc. Can., Program Abstr.* **26**, 65.

_____, RUDNICK, R.L. & MCDONOUGH, W.F. (2000): Precise elemental and isotope ratio determination by simultaneous solution nebulization and laser ablation – ICP – MS: application to U–Pb geochronology. *Chem. Geol.* **164**, 281-301.

HORSTWOOD, M.S.A., FOSTER, G.L., PARRISH, R.R. & NOBLE, S.R. (2001): Common-Pb and inter-element corrected U–Pb geochronology by LA–MC–ICP–MS. *Eleventh Goldschmidt Conf., Abstr.* **3698**.

JACKSON, S.E. (2001): The application of Nd:YAG lasers in LA–ICP–MS. *In* Laser-Ablation – ICPMS in the Earth Sciences: Principles and Applications (P. Sylvester, ed.). *Mineral. Assoc. Can., Short Course* **29**, 29-47.

_____, HORN, I., LONGERICH, H.P. & DUNNING G.R. (1996): The application of laser ablation microprobe (LAM) – ICP – MS to in situ U–Pb zircon geochronology. *V.M. Goldschmidt Conf., J. Conf. Abstr.* **1**, 283.

_____, LONGERICH, H.P., DUNNING, G.R. & FRYER, B.J. (1992): The application of laser-ablation microprobe – inductively coupled plasma – mass spectrometry (LAM–ICP–MS) to *in situ* trace element determinations in minerals. *Can. Mineral.* **30**, 1049-1064.

JEFFRIES, T.E., JACKSON, S.E. & LONGERICH, H.P. (1998): Application of a frequency quintupled Nd:YAG source (λ 213 nm) for laser ablation inductively coupled plasma mass spectrometric analysis of minerals. *J. Anal. At. Spectrom.* **13**, 935-940.

KETCHUM, J.W.F, JACKSON, S.E., CULSHAW, N.G. & BARR, S.M. (2001): Depositional and tectonic setting of the Paleoproterozoic Lower Aillik Group, Makkovik Province, Canada: evolution of a passive margin – foredeep sequence based on petrochemistry and U–Pb (TIMS and LAM–ICP–MS) geochronology. *Precamb. Res.* **105**, 331-356.

LI, XIANHUA, LIANG, XIRONG, SUN, MIN, GUAN, HONG & MALPAS, J.G. (2001): Precise $^{206}Pb/^{238}U$ age determination on zircons by laser ablation microprobe – inductively coupled plasma – mass spectrometry using continuous linear ablation. *Chem. Geol.* **175**, 209-219.

LONGERICH, H.P., GÜNTHER, D. & JACKSON, S.E. (1996b): Elemental fractionation in laser ablation inductively coupled plasma mass spectrometry. *Fresenius J. Anal. Chem.* **355**, 538-542.

_____, JACKSON, S.E. & GÜNTHER, D. (1996): Laser ablation inductively coupled plasma mass spectrometric transient signal data acquisition and analyte concentration calculation. *J. Anal. At. Spectrom.* **11**, 899-904.

MANK, A.J.G. & MASON, P.R.D. (1999): A critical assessment of laser ablation ICP–MS as an analytical tool for depth analysis in silica-based glass samples. *J. Anal. At. Spectrom.* **14**, 1143-1153.

NORMAN, M.D., PEARSON, N.J., SHARMA, A. & GRIFFIN, W.L. (1996): Quantitative analysis of trace elements in geological materials by laser ablation ICPMS: instrumental operating conditions and calibration values of NIST glasses. *Geostandards Newsletter* **20**, 247-261.

VAN ACHTERBERGH, E., RYAN, C.G. & GRIFFIN, W.L. (1999): Glitter: on-line interactive data reduction for the laser ablation ICP–MS microprobe. *Proc. 9th V.M. Goldschmidt Conf.* (*Boston*).

WIEDENBECK, M., ALLE, P., CORFU, F., GRIFFIN, W.L., MEIER, M., OBERLI, F., VON QUADT, A., RODDICK, J.C. & SPIEGEL, W. (1995): Three natural zircon standards for U–Th–Pb, Lu–Hf, trace elements and REE analyses. *Geostandards Newsletter* **19**, 1-23.

WILLIAMS, I.S. (1998): U–Th–Pb geochronology by ion microprobe. *In* Application of Microanalytical Techniques to Understanding Mineralizing Processes (M.A. McKibben, W.C. Shanks III & W.I. Ridley, eds.). *Rev. Econ. Geol.* **7**, 1-35.

Received October 1, 2001, revised manuscript accepted July 27, 2002.